Cell Research (2011) 21:1295-1304.
© 2011 IBCB, SIBS, CAS All rights reserved 1001-0602/11 $ 32.00
www.nature.com/cr

ORIGINAL ARTICLE

Imaging superoxide flash and metabolism-coupled mitochondrial permeability transition in living animals

Huaqiang Fang[1, 2, *], Min Chen[1, *], Yi Ding[1, *], Wei Shang[1], Jiejia Xu[1], Xing Zhang[3], Wanrui Zhang[1], Kaitao Li[1], Yao Xiao[1], Feng Gao[3], Shujiang Shang[1], Jing-Chao Li[2], Xiao-Li Tian[1], Shi-Qiang Wang[2], Jingsong Zhou[4], Noah Weisleder[5], Jianjie Ma[5], Kunfu Ouyang[6], Ju Chen[6], Xianhua Wang[1], Ming Zheng[1], Wang Wang[7], Xiuqin Zhang[1], Heping Cheng[1, 2]

[1]Institute of Molecular Medicine, College of Life Science, Peking University, Beijing 100871, China; [2]State Key Laboratory of Biomembrane and Membrane Biotechnology, College of Life Science, Peking University, Beijing 100871, China; [3]Department of Physiology, The Fourth Military Medical University, Xi'an 710023, China; [4]Department of Molecular Biophysics and Physiology, Rush University School of Medicine, Chicago, IL 60612, USA; [5]Department of Physiology and Biophysics, Robert Wood Johnson Medical School, Piscataway, NJ 08854, USA; [6]Department of Medicine, University of California, San Diego, CA 92093, USA; [7]Mitochondria and Metabolism Center, Department of Anesthesiology and Pain Medicine, University of Washington, Seattle, WA 98109, USA

The mitochondrion is essential for energy metabolism and production of reactive oxygen species (ROS). In intact cells, respiratory mitochondria exhibit spontaneous "superoxide flashes", the quantal ROS-producing events consequential to transient mitochondrial permeability transition (tMPT). Here we perform the first *in vivo* imaging of mitochondrial superoxide flashes and tMPT activity in living mice expressing the superoxide biosensor mt-cpYFP, and demonstrate their coupling to whole-body glucose metabolism. Robust tMPT/superoxide flash activity occurred in skeletal muscle and sciatic nerve of anesthetized transgenic mice. In skeletal muscle, imaging tMPT/superoxide flashes revealed labyrinthine three-dimensional networks of mitochondria that operate synchronously. The tMPT/superoxide flash activity surged in response to systemic glucose challenge or insulin stimulation, in an apparently frequency-modulated manner and involving also a shift in the gating mode of tMPT. Thus, *in vivo* imaging of tMPT-dependent mitochondrial ROS signals and the discovery of the metabolism-tMPT-superoxide flash coupling mark important technological and conceptual advances for the study of mitochondrial function and ROS signaling in health and disease.

***Keywords*:** reactive oxygen species; mitochondrial permeability transition; energy metabolism; *in vivo* molecular imaging
Cell Research (2011) **21**:1295-1304. doi:10.1038/cr.2011.81; published online 10 May 2011

Introduction

Reactive oxygen species (ROS) are bioactive molecules playing multifunctional roles in cell physiology and pathophysiology. Imbalanced ROS signals due to exaggerated ROS production or deficient ROS removal are widely recognized as pathogenic factors in a large panel of metabolic, cardiovascular and neurodegenerative diseases [1-3]. However, low levels of ROS are emerging as versatile messengers indispensable to vital physiological processes ranging from signal transduction, gene expression, development and wound healing [4-6]. Of many intracellular ROS production mechanisms, the mitochondrion is the most prominent ROS generator wherein constitutive ROS production arises from leakage of a small percent of electrons from the electron transfer chain (ETC) [7, 8]. In skeletal muscle, which requires high energy supply and contains abundant mitochondria, adequate amount of ROS modulates muscle contractility and glucose metabolism [9, 10], while excessive ROS is responsible for muscle fatigue and insulin resistance [1,

*These three authors contributed equally to this work.
Correspondence: Heping Cheng[a], Xiuqin Zhang[b]
[a]E-mail: chengp@pku.edu.cn
[b]E-mail: zhangxq@pku.edu.cn
Received 9 February 2011; revised 21 March 2011; accepted 24 March 2011; published online 10 May 2011

11, 12].

Until now, much of our understanding of mitochondrial ROS production and its regulation during energy metabolism has been based on experiments in isolated mitochondria and fragmented mitochondrial preparations, much less in intact cells and little at the organism level. A confounding factor has been the lack of means for detection of mitochondrial ROS dynamics in truly integrative physiological context. For instance, the wildly used intracellular ROS probe dichlorofluorescein suffers critical limitations, including inability for specific targeting into mitochondria in cells, poor selectivity among ROS species, and generation of ROS by itself on illumination [13], while the mitochondria-specific and superoxide-selective probe dihydroethidium (Mito-HE or MitoSOX red) is limited by its irreversible ROS-reactive kinetics, rendering its low temporal resolution [14].

Recently we reported a serendipitous finding that a circularly permuted yellow fluorescent protein (cpYFP) is a novel genetically encoded indicator highly selective for superoxide anions, with sensitivity and kinetic properties suitable for real-time tracking of superoxide production. By targeting cpYFP into the matrix of mitochondria, we discovered a new mode of mitochondrial superoxide production in which mitochondria intermittently undergo transient permeability transition (tMPT) and consequently generate quantal bursts of superoxide anions, termed "superoxide flashes" [15]. Such tMPT-regulated ROS production requires functioning ETC, as is the case with constitutive ROS production mentioned above. It has been shown that superoxide flashes occur universally in all types of cells and tissues examined, including cultured neurons, isolated cardiac and skeletal muscle cells, and intact heart under the Langendorff perfusion [15, 16]. During hypoxia/reoxygenation injury in cultured cardiac myocytes, tMPT/superoxide flash frequency increases in a time window between 5 to 15 min after reperfusion, contributing to the oxidative stress [15]. This breakthrough holds the promise of investigating mitochondrial ROS signals in the truly physiological and integrating context of intact organism.

The primary goal of this study was to develop appropriate animal models and novel imaging techniques that fulfill the promise of measuring single-mitochondrion ROS dynamics *in vivo*. Specifically, we visualized mitochondrial tMPT and superoxide flash activity in multiple tissues, including sciatic nerve trunk and skeletal muscle in anesthetized mice expressing mitochondrially targeted cpYFP (mt-cpYFP). Imaging tMPT/superoxide flash activity during whole-body metabolic stimulation revealed a tight coupling between tMPT-dependent ROS production and mitochondrial energy metabolism in living animals. Thus, *in vivo* imaging of tMPT/superoxide flash activity provides a unique and timely technology that could be widely applicable for the investigation of physiological and pathophysiological mitochondrial ROS signaling in living animals.

Results

Pan-tissue mt-cpYFP transgenic mice

To measure mitochondrial superoxide signals *in vivo*, we first generated transgenic mice expressing mt-cpYFP driven by the chicken β-actin promoter (Figure 1A, and Supplementary information, Figure S1A). Pan-tissue expression of mt-cpYFP was confirmed by RT-PCR analysis (Supplementary information, Figure S1B). Confocal microscopy revealed intense mt-cpYFP fluorescence in the myocardium, skeletal muscle and sciatic nerve trunk of transgenic mice (Figure 1B-1D), while autofluorescence in corresponding tissues from wild type animals was negligible under the same detection conditions (data not shown). Histological analysis by hematoxylin/eosin staining revealed no discernible abnormalities in tissues and cell structures (Supplementary information, Figure S2A), nor were there significant changes in heart and body weight, or their ratio in adult transgenic mice (Supplementary information, Figure S2B).

The subcellular distribution of mt-cpYFP shows tissue-specific patterns that are consistent with mitochondrial matrix targeting of the superoxide indicator. Fluorescent cardiac mitochondria were observed between the Z-lines of sarcomeres and arranged as longitudinal bundles along the myofibrils (Figure 1B) [17, 18]. In skeletal muscle, mt-cpYFP staining of I band-delimited mitochondria [18, 19] gave rise to transverse doublet bands at 2.6 μm intervals (Figure 1C) that overlapped with staining by tetramethylrhodamine methyl ester (TMRM), a mitochondrial membrane potential ($\Delta\Psi m$) indicator (Supplementary information, Figure S3). Unlike striated muscles, axons within the sciatic nerve trunk were filled with slender mitochondria (Figure 1D), many of which were engaged in anterograde or retrograde trafficking. This pattern is in agreement with a previous report on mitochondrial morphology and motility in nerve fibers [20].

Visualizing tMPT/superoxide flashes in multiple tissues of living animals

We next developed an imaging procedure for real-time measurement of tMPT/superoxide flashes in anesthetized transgenic mice bearing the superoxide indicator (Figure 2A). High-resolution imaging of surgically exposed gastrocnemius muscle or sciatic nerve trunk was achieved

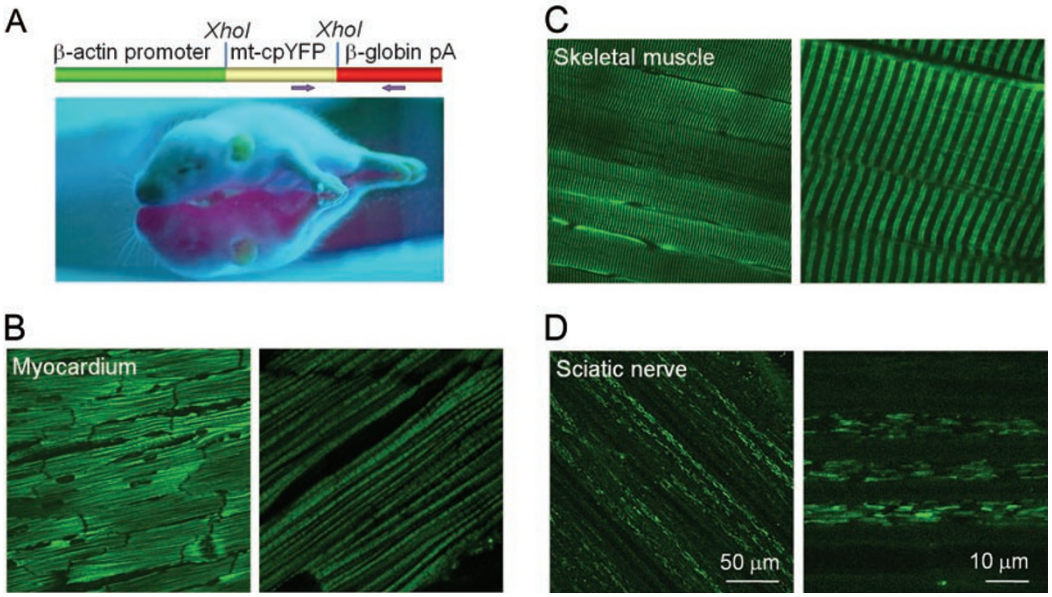

Figure 1 Pan-tissue expression of mt-cpYFP in transgenic mice. **(A)** A neonatal *mt-cpYFP* transgenic mouse under UV illumination. Top: plasmid construct for generating the transgenic mouse. The full-length *mt-cpYFP* DNA was cloned into pUC-CAGGS vector downstream of the chicken β-actin promoter. Arrows indicate the positions of forward and backward primers for genotyping. **(B-D)** Confocal images of mt-cpYFP fluorescence in myocardium **(B)**, gastrocnemius muscle **(C)** and sciatic nerve trunk **(D)** at low and high magnifications. Note the cell type-specific pattern of intracellular mitochondrial distribution. **(B-D)** use the same scale bar in **D**.

with either an upright or inverted laser scanning confocal microscope operating in a 2D (*xy*), 3D (*xy-t*) or 4D (*xyz-t*) configuration (see Materials and Methods). Figure 2B and Supplementary information, Video S1 show a representative tMPT/superoxide flash occurring spontaneously at an I-band, ~30 μm beneath the surface of a gastrocnemius muscle fiber. Such elemental events rose to a peak $\Delta F/F_0$ of 0.51 ± 0.06 (n = 68; Figure 2C), lasted 9.15 ± 0.63 s (full duration at half amplitude, FDHM) and occupied an area of only 0.54 ± 0.03 μm^2 (full area at half amplitude, FAHM), the size of one or a small number of tightly packed mitochondria. Spontaneous tMPT/superoxide flashes were also detected in axons of sciatic nerve trunk, with all events (n = 24) found in stationary but not traveling mitochondria (Figure 2D, Supplementary information, Video S2). This observation is in line with previous reports and indicates that stationary mitochondria are actively respiring and providing ATP for local function [21, 22], whereas mitochondria during transportation are either immature or inactive in energy metabolism. While differing in morphology, neuronal and skeletal muscle tMPT/superoxide flashes shared many common features, both displaying mean amplitude of 0.5, time to peak of 5 s and half decay times of 6 s (Figure 2C). These *in vivo* superoxide flashes are also highly comparable with those in cells [15, 16] and in isolated hearts from pan-tissue (Supplementary information, Figure S4) or cardiac-specific mt-cpYFP transgenic mice [15]. The occurrence of spontaneous superoxide flashes in multiple tissues of living animals suggests that tMPT-dependent quantal ROS production is a universal and physiological process of mitochondria functioning *in vivo*.

Imaging tMPT/superoxide flashes revealed functional mitochondrial network in vivo

Apart from single-mitochondrion events, *in vivo* imaging of tMPT/superoxide flash activity uncovered extensive functional mitochondrial networks in skeletal muscle. Arrays of neighboring mitochondria along the same or a few neighboring I-bands would ignite and extinguish synchronously, giving rise to either a linear (length > 2 μm) or lamellar (≥ 2 sarcomeres) appearance in *xy* optical sections (Figure 2E and 2F). Quantitatively, about 65% of the total events were categorized as punctiform and 35% as synchronized (linear or lamellar) superoxide flashes (Supplementary information, Figure S5). Simultaneous monitoring of the TMRM fluorescence showed that synchronized superoxide flashes were accompanied by transient depolarization of membrane potential (loss of $\Delta\Psi m$, an indication of MPT opening; Figure 2F and

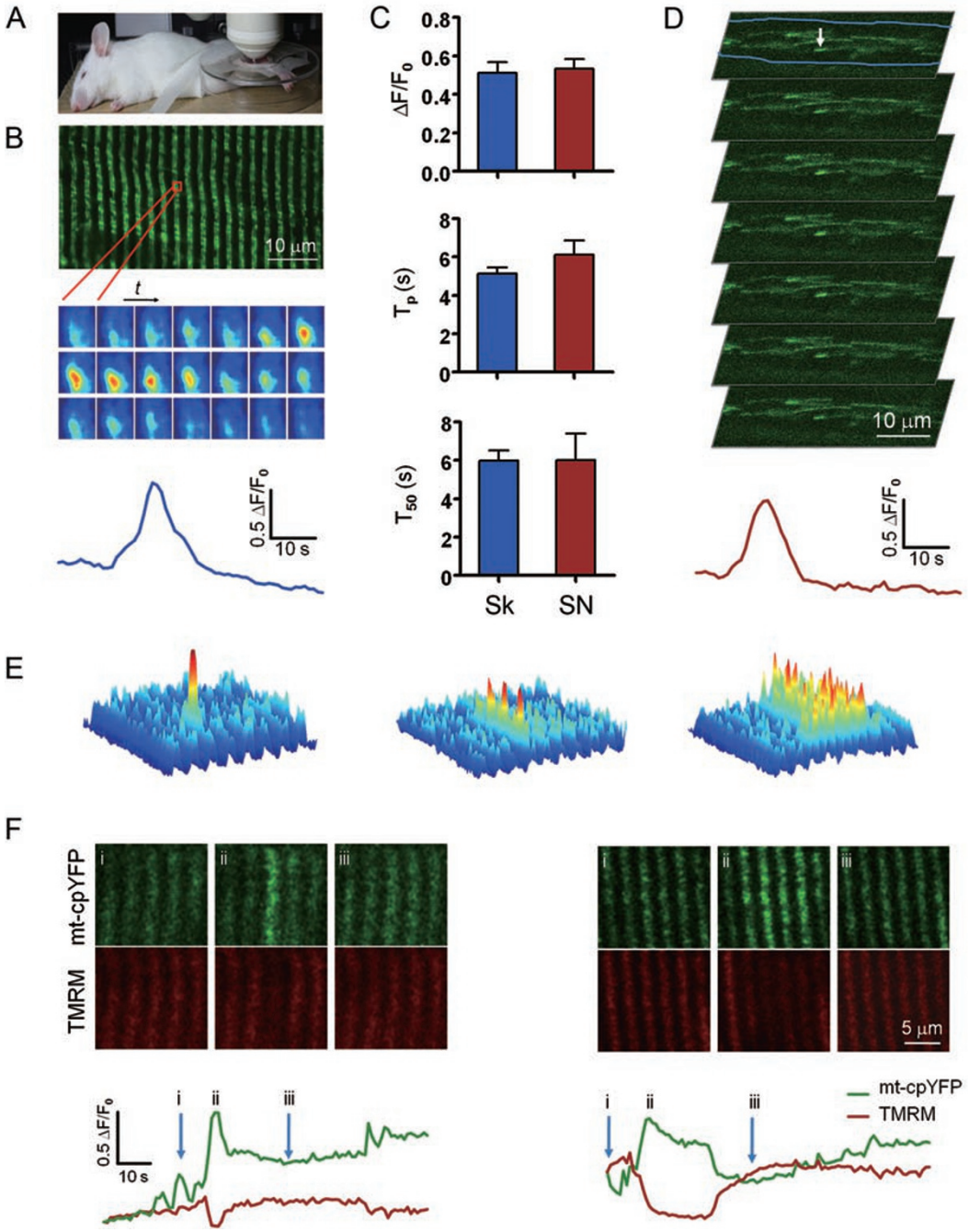

Figure 2 Imaging tMPT/superoxide flashes in living mice. **(A)** *In vivo* imaging of a *mt-cpYFP* transgenic mouse under anesthesia. An upright confocal microscope was used to image hind limb skeletal muscle and sciatic nerve trunks exposed after skin incision. **(B)** Punctiform tMPT/superoxide flashes in mouse gastrocnemius. From top to bottom: *xy* view of mitochondria in doublet bands flanking the z-lines; time lapse, enlarged views of the flash in a boxed region of 1.57 μm × 1.76 μm; and time course plot of the superoxide flash. **(C)** Characteristics of skeletal muscle (Sk) and sciatic nerve (SN) superoxide flashes. $\Delta F/F_0$, amplitude; T_p, time to peak; T_{50}, half decay time. **(D)** Time-lapse images and time course plot of a tMPT/superoxide flash in an axon (outlined in blue) of sciatic nerve trunk. The arrow marks the mitochondrion undergoing excitation. **(E)** Surface plots showing punctiform (left), linear (middle) and lamellar (right) tMPT/superoxide flashes in gastrocnemius. **(F)** Transient loss of $\Delta\Psi m$ (indexed by TMRM signal) during synchronized tMPT/superoxide flashes (the same as those in **E**). Similar results were obtained in four other fibers.

Supplementary information, Video S3), suggesting that tMPT serves as the common trigger mechanism of synchronized and single mitochondrial superoxide flashes [15]. Indeed, synchronized superoxide flashes were indistinguishable from punctiform ones by virtue of amplitude and kinetics (Supplementary information, Figure S5) despite their distinctive morphology.

To determine the degree of synchrony during excitation of a functional mitochondrial network, we performed 3D (*xy*-*t*) imaging at five frames/s. A representative example is shown in Figure 3A. This event spanned 6.4 μm transversely and 5.7 μm longitudinally, encompassing three sarcomeres; yet, space-time plots (*xt* and *yt*) reconstructed from the *xy*-*t* image stack showed that all parts of the functional network are activated simultaneously (within the limit of temporal resolution), indicating that the network behaves as if it was a single physical unit. To delineate the three-dimensional (3D) geometry of such mitochondrial network, we applied 4D (*xyz*-*t*) imaging technique to acquire *xyz* stacks at 2.37 s per stack of 10 optical sections at 1 μm *z*-intervals (Figure 3B). Reconstruction from the 4D image data set portrayed the shape of synchronized tMPT/superoxide flash as a labyrinthine mitochondrial network in three dimensions (Figure 3C). On certain *z*-planes, elongated mitochondrial elements ran in the longitudinal direction and appeared to connect the mitochondria at I-bands of two or more sarcomeres (Figure 3B, 3C and Supplementary information, Video S4). Furthermore, the longitudinal mitochondrial elements were also evident in quiescent cells (Supplementary information, Figure S6). This suggests that physical connectivity underlies functional integration of the local mitochondrial network.

Imaging tMPT/superoxide flash activity during altered oxidative metabolism

Previous studies have shown that tMPT/superoxide flash production depends on active respiration of the mi-

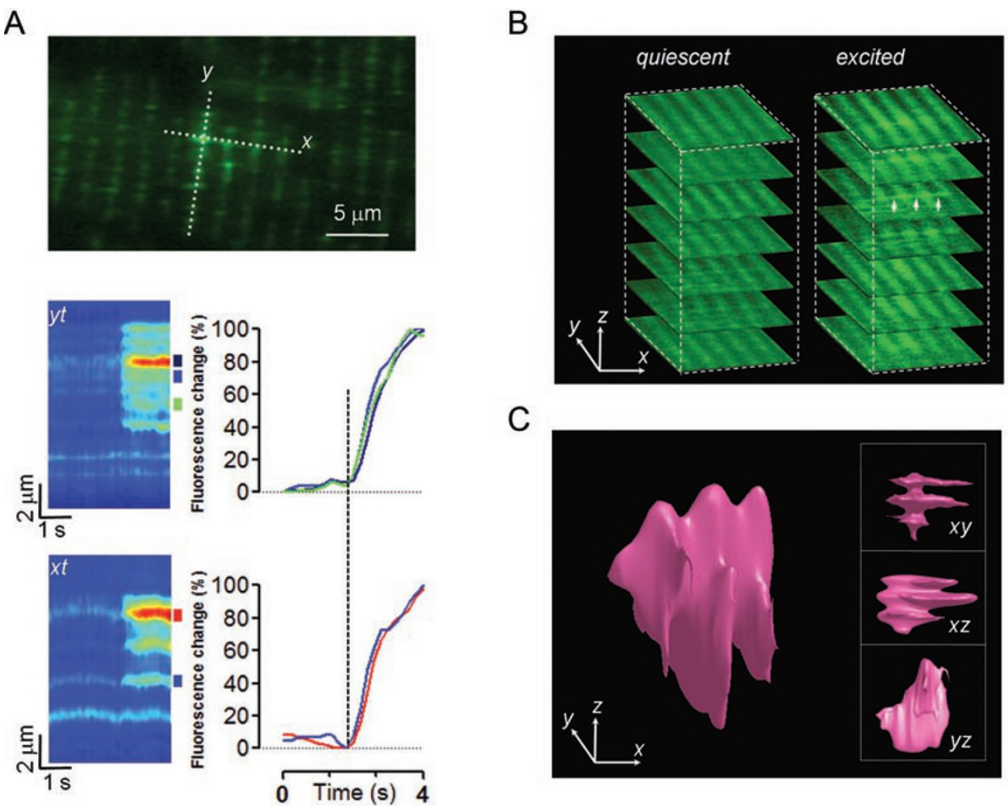

Figure 3 Synchrony and geometry of functional mitochondrial network in skeletal muscle. **(A)** Synchrony in a lamellar tMPT/superoxide flash. Data are shown as *xy* view (top) and space-time plots along the transverse (*yt*) and longitudinal (*xt*) directions of the flash. Line plots show the rising phase of the flash (normalized by respective amplitude) at locations marked by colored bars flanking the space-time plots. Dashed line marks the simultaneous take-off of the flash. **(B)** Synchronized tMPT/superoxide flash in *xyz* stack. Subset *z*-stacks corresponding to quiescent and excited states of a functional network. Arrowheads mark longitudinal elements on a *z*-plane of the network. **(C)** Three-dimensional views of the boundary of the network in **B**. See Materials and Methods for details of digital reconstruction and Supplementary information, Video S4 for animation.

tochondria in intact cells [15]. The *in vivo* mitochondrial ROS imaging technique described above provides an unprecedented opportunity to test whether tMPT-dependent ROS signals are coupled to mitochondrial energy metabolism at the whole animal level. Because skeletal muscles are responsible for 70-90% of insulin-stimulated glucose clearance [23, 24] and play a prominent role in the development of metabolic disorders, we opted to use gastrocnemius muscle to track tMPT/superoxide flash activity while varying whole-body metabolic status (Figure 4A). Intraperitoneal injection of glucose (2 g/kg body weight) resulted in a time-dependent rise in the plasma glucose level within 30 min, followed by a gradual clearance (Supplementary information, Figure S7A) as observed previously [25]. *In vivo* imaging revealed that tMPT/superoxide flash activity surged, with a ~3.0-fold increase between 30 to 90 min after glucose administration (Figure 4A, 4B). Intraperitoneal injection of insulin (1 U/kg), which stimulates glucose transportation and utilization by skeletal muscles [23], profoundly lowered plasma glucose level (Supplementary information, Figure S7B) while causing a similar surge in tMPT/superoxide flash activity (Figure 4A and 4C). These data indicate that skeletal muscle tMPT/superoxide flash production is closely associated with mitochondrial energy metabolism in living animals.

We further characterized and compared unitary properties of tMPT/superoxide flashes under different metabolic conditions. The amplitude and FDHM of basal tMPT/superoxide flashes exhibited broad distributions (Figure 4D and 4E), the variability of which could be attributed to multiple determinants including ETC activity, tMPT

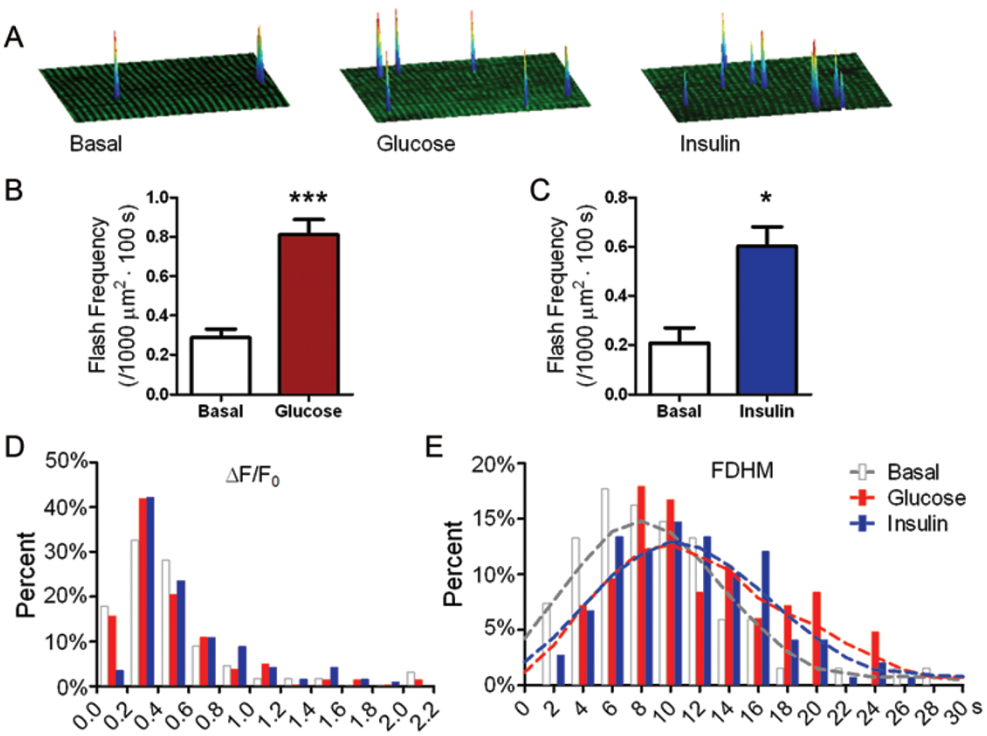

Figure 4 Decoding metabolic status by the frequency of tMPT/superoxide flashes. **(A)** Representative examples showing tMPT/superoxide flash activities in basal conditions and after glucose or insulin challenges in different *mt-cpYFP* transgenic mice. Data are presented as overlay of *xy* view of a region of gastrocnemius muscle under study (bottom) and surface plot of all superoxide flashes combined from a 100-s data set. **(B**, **C)** tMPT/superoxide flash activity (column bars) during glucose (**B**, 2 g/kg body weight, n = 9 mice) or insulin challenge (**C**, 1 U/kg body weight, n = 6 mice). **(D**, **E)** Histogram analysis of unitary properties of superoxide flashes. F/F_0, amplitude; FDHM: full duration at half maximum. The traces represent nonlinear least square fittings to the FDHM histograms with multiple Gaussian functions $f(x) = a_1 \exp\left(-\frac{(x-\mu_1)^2}{\sigma_1^2}\right) + a_2 \exp\left(-\frac{(x-\mu_2)^2}{\sigma_2^2}\right)$ and data from all three groups were constrained simultaneously, yielding μ_1 = 7.5, μ_2 = 14, σ_1 = 4.9 and σ_2 = 7.1. The individual component ratio was a_1:a_2 = 17.3:3.6, 9.6:9.1 or 10.5:8.3 for basal, glucose or insulin group, respectively. n = 68-150 events from 4-6 mice. *P < 0.05, **P < 0.01, ***P < 0.001 versus basal.

duration and the relative location to the focal plane. Multiple Gaussian fitting to the FDHM histogram revealed a major component centered at 7.5 s (mode 1 gating) and a minor component at 14 s (mode 2 gating). Remarkably, the amplitude histogram distribution of tMPT/superoxide flashes was essentially unaffected by glucose or insulin challenge (Figure 4D). The relative abundance of punctiform versus synchronized flashes was also similar regardless of metabolic status (Supplementary information, Figure S5), indicating that punctiform and network mitochondria respond similarly to metabolic stimulation. The FDHM histogram analysis, however, showed an increase in mode 2 gating component (Figure 4E), rendering 40% or 33% increase in mean value after glucose or insulin challenge, respectively. These results suggest that tMPT/superoxide flashes decode metabolic status, in a frequency-modulated (FM) manner and involving also a shift in the gating mode of mitochondrial permeability transition pore (mPTP).

Discussion

As mitochondria and ROS regain the central stage of biomedicine, investigation of mitochondrial ROS signaling is significantly hinged on the development of new ROS detection technology applicable to truly physiological and integrative conditions. The aim of this study was thus to develop a molecular imaging method for real-time measurement of mitochondrial ROS in living animals at the single mitochondrion resolution. To this end, we used the newly developed superoxide-selective indicator mt-cpYFP to generate indicator-expressing transgenic mouse lines, and developed novel *in vivo* imaging techniques that enabled real-time investigation of tMPT/superoxide flash in multiple tissues of anesthetized mice under different experimental settings. Specifically, we visualized the production of tMPT/superoxide flashes in skeletal muscles and sciatic nerves of living mice, correlated mitochondrial ROS bursts with loss of $\Delta\Psi m$, characterized tissue-specific tMPT/superoxide flash properties, and revealed robust responses of tMPT/superoxide flash activity to altered metabolic status.

Unlike cardiac and neuronal tMPT/superoxide flashes that are confined to punctiform and linear mitochondria, events in skeletal muscle are highly heterogeneous in shape and size, manifesting punctiform, linear or lamellar appearance as seen in the confocal optical sections. Several lines of evidence indicate that synchronized (linear or lamellar) tMPT/superoxide flashes reflect the excitation of networking mitochondria. First, ultrafast *xy-t* 3D imaging demonstrated that all parts of a spatially extended event are excited and extinguished synchronously. Second, ultrafast *xyz-t* 4D imaging, to portray the event's morphology in 3D, showed that mitochondria within the boundary of labyrinthine tMPT/superoxide flashes are physically connected, and the connectivity between neighboring sarcomeres appears to be mediated by filamentous mitochondrial elements that run longitudinally. Functional characterization further revealed that both punctiform and synchronized events display stereotypical amplitude and kinetics and their relative abundance remains unchanged during metabolic perturbations and oxidative stress. This result is in favor of structural rather than functional heterogeneity as the cause of diverse spatial patterns of tMPT/superoxide flashes. Taken together, these data strongly support a working model of local mitochondria networks in which all participant mitochondria are physically connected, and operate synchronously in an all-or-none manner. That synchronized tMPT/superoxide flashes account for 1/3 of total events further suggests that mitochondrial networking is a common phenomenon in adult skeletal muscle. This finding is in contrast to the apparent lack of mitochondrial mobility and hence active fusion and fission (during the period of hour-long observation). Nevertheless, it is in good agreement with classical electron microscopy studies that have revealed the existence of reticulum-like, 3D mitochondrial networks [19] or inter-mitochondrial connections via filamentous elements in skeletal muscle [26, 27].

Our *in vivo* imaging method has enabled us to investigate, for the first time, single mitochondrial behavior in living animals when whole-body metabolism is perturbed. This approach has led to the demonstration of the coupling between mitochondrial metabolism and tMPT/superoxide flash activity in living animals: The frequency of tMPT/superoxide flashes increases in response to systemic administration of glucose or insulin, with only marginal alterations of unitary properties and no change in proportions of punctiform, linear or lamellar events. It should be emphasized that the metabolism-flash coupling differs from conventional view of ETC-coupled ROS production, in two important ways. First, it invokes tMPT activity, while both modes of ROS production require electron leakage from the ETC. Second, it operates in an intermittent, all-or-none manner. As such, the superoxide flashes decode mitochondrial metabolism in an apparent FM manner. The concurrent change in the flash kinetics also suggests the involvement of a shift in the gating mode of mPTP. That tMPT and superoxide flashes are robust, house-keeping events *in vivo* provides unequivocal evidence that they are a truly elemental physiological process, in contrast to the notion that sustained MPT signifies the commitment of the cell fate to

apoptosis [7, 28].

Since tMPT allows for rapid equilibrium of small molecules between the mitochondrial matrix and the cytosol [29] and ROS regulate the activity of many kinases (e.g., insulin receptor/tyrosine kinase and Ca^{2+}-calmodulin kinase II) [30, 31] and phosphatases (e.g., protein tyrosine phosphatases) [4, 32] that participate in energy metabolism, it is conceivable that FM control of the intermittent tMPT activity provides an efficient means for feedback regulation of metabolism (e.g., coordination of substrate and product transport across the inner mitochondrial membrane, regulation of the rate of intermediary metabolic reactions). Alternatively, it may represent a feed-forward mechanism for coordination between energy metabolism and local ROS signaling.

In summary, live animal imaging of superoxide biosensor-expressing mice has shown that tMPT and superoxide flashes are robust, house-keeping events *in vivo*. With this new technical advance, we have uncovered the coupling between energy metabolism and tMPT-dependent quantal ROS production. These findings invite extension and revision of current theories on the function of MPT and the mode of mitochondrial ROS production. We envision that our novel technology will be widely applicable to delineating role of mitochondria in the pathogenesis of metabolic disorders (e.g., obesity and diabetes mellitus) and oxidative stress-related diseases (e.g., cancer, heart failure and neurodegeneration). In preclinical settings, it may also be used for direct assessment of mitochondrial responses to medicinal, cell and gene therapies in living animals.

Materials and Methods

Generation of mt-cpYFP transgenic mice

To generate pan-tissue transgenic mice expressing mt-cpYFP, full-length *mt-cpYFP* DNA was cloned into the *Xho*I site of pUC-CAGGS vector downstream of chicken β-actin promoter. The construct was linearized with NotI, purified with a DNA purification kit (Qiagen), and microinjected into fertilized eggs of ICR (Institute of Cancer Research) mice. The transgenic mice were kept on a 12-h light cycle; food and water were provided *ad libitum*. Mice of both genders at the age of 8-12 weeks were used for live animal imaging. All protocols were approved by the Institutional Animal Care and Use Committee of Peking University accredited by AAALAC International.

Genotyping, RT-PCR and histology

Mouse-tail DNA was isolated with a genomic DNA isolation kit. Genotyping was performed by PCR with a forward primer within mt-cpYFP cDNA (5′-GCACAAGCTGGAGTACAACGGT-3′) and a reverse primer within β-globin poly (A) (5′-GATGACCTCTTTATAGCCAACCT-3′), giving rise to a 394 bp fragment. Internal control, a 530 bp *Gapdh* fragment, was amplified with a forward primer (5′-AGGCCGGTGCTGAGTATGTC-3′) and a reverse primer (5′-TGCCTGCTTCACCACCTTCT-3′). RT-PCR was used to analyze mt-cpYFP mRNA levels in multiple tissues of 2-month-old transgenic mice. Total RNA was extracted from snap-frozen tissues with Trizol (Invitrogen) and a 2 μg of RNA was used to generate cDNA by using M-MLV RTase (Takara). The specific primers were *mt-cpYFP*: forward 5′-AGTCACTATAGGGAGACCCAAGC-3′, reverse 5′-GACTGGAAGCTCAGGTAGTGGTT-3′, with a 273 bp fragment; *18s* rRNA: forward 5′-GGAAGGGCACCACCAGGAGT-3′, reverse 5′-TGCAGCCCCGGA CATCTAAG-3′, with a 316 bp fragment.

For histological study, anesthetized mice were sequentially perfused with PBS and 4% paraformaldehyde through a syringe inserted into the left ventricle, and the right atrial appendage was cut open for drainage. Following perfusion, organs and tissues were removed and kept in 4% paraformaldehyde for 16 h. The fixed tissues were embedded in paraffin, sectioned at 8 μm and stained with hematoxylin and eosin. Images were taken with a light microscope (Olympus).

Multidimensional confocal imaging in vivo

Mice were anesthetized with pentobarbital sodium (80 mg/kg body weight) by intraperitoneal injection and placed in a custom-devised chamber. Sterile ophthalmic ointment was placed in each eye. Skin at the surgical area was shaved and prepared for sterile surgery with 70% alcohol. An incision was made at the medial side of one hindlimb to expose the gastrocnemius muscle or sciatic nerve trunk. Either an inverted (Zeiss LSM 710) or an upright confocal microscope (Zeiss LSM 700) was used to detect superoxide flashes while exposed tissues were immersed in isotonic balanced salt solution containing (in mM): 140 NaCl, 5 KCl, 2.5 $CaCl_2$, 2 $MgCl_2$ and 10 HEPES (pH 7.2). Mice were placed on isothermo pads to maintain a constant body and muscle temperature. Two-dimensional (2D, *xy*) confocal images were recorded using a 40× 1.0 numerical aperture water-immersion lens in the upright configuration or a 40× 1.3 numerical aperture oil-immersion lens in the inverted configuration. Fast time-lapse 3D (*xy-t*) or 4D (*xyz-t*) images were recorded using a 40× 1.3 numerical aperture oil-immersion lens (Zeiss LSM 510 Live, inverted configuration). The focal plane was set < 50 μm from the tissue surface and the axial resolution was set at 1.0 μm. Dual wavelength excitation imaging of mt-cpYFP was achieved by alternating excitation at 405 and 488 nm and detecting emission at > 505 nm. Triple wavelength excitation imaging of mt-cpYFP and TMRM was achieved by tandem excitation at 405, 488 and 543 nm, and the emission was detected at 505-530, 505-530 and > 560 nm, respectively. For *in vivo* loading of TMRM into the skeletal muscle, extracellular solution containing 500 nM TMRM was topically applied to the incision-exposed skeletal muscle for 30 min and then washed out with TMRM-free solution. Time-lapse images (*xy-t*) were taken at 1-s intervals. Ten z-planes, each with alternating 405 and 488 nm excitation, of a *z*-stack were taken at 1 μm intervals every 2.37 s. The intensity of each pixel was digitized at 8-bit depth.

Detection of tMPT/superoxide flashes during metabolic manipulations

For glucose challenge, *mt-cpYFP* transgenic mice were fasted for 6-12 hr with free access to water. Anesthetized mice were injected intraperitoneally with 2 g/kg body weight glucose. Blood was collected at 0, 5, 15, 30, 45 and 60 min after injection, and

glycaemia was determined by a portable glucometer (ACCU CHEK Advantage, Roche). For insulin challenge, anesthetized mice under random-fed conditions were intraperitoneally injected with 1 U/kg body weight insulin (Sigma) diluted in sterile saline. Blood samples were collected at 0, 5, 15, 30, 45, 60 and 75 min for glycaemia analysis. The tMPT/superoxide flash activity was monitored over time windows of 20-50 min before and 30-90 min after metabolic manipulation, in randomly selected fibers of gastrocnemius, with 100 *xy* images taken in 100 s at each site of 70.8 $\times$ 44.3 μm^2.

Image processing and superoxide flash analysis

Confocal images were analyzed using custom-developed programs written in Interactive Data Language (IDL, Research Systems). Cell motion and contraction artifacts were largely corrected by image processing such that the same cellular structures in different frames were aligned for parametric measurement and data presentation. This correction was guided by the 405 nm excitation images, which showed no changes during tMPT/superoxide flashes, and were omitted from figure presentation for simplicity. Individual superoxide flashes were identified with the aid of custom-devised computer algorithms, and their morphological and kinetic properties, including amplitude ($\Delta F/F_0$, maximum fluorescence increase over baseline), time to peak (T_p), half decay time (T_{50}), FDHM and FAHM, were measured automatically.

To delineate the 3D boundary of a tMPT/superoxide flash from 4D *xyz-t* stacks, the raw *xyz* stacks were first rotated about the *z*-axis for a proper viewpoint, using bilinear interpolation for this geometric transformation. Then, a rectangular volume encompassing a tMPT/superoxide flash was selected and subjected to singular value decomposition to perform principal component analysis in order to decrease the interference of the noise. By taking about 70% of all the components to reconstruct the image with reduced noise and further smoothing with the Gaussian blur method; the interval volume tetrahedrization method provided by IDL was used to generate a tetrahedral mesh from selected volumetric data (e.g., *xyz* stack at the peak of a tMPT/superoxide flash).

Statistical analysis

Results are expressed as mean ± s.e.m. Student's *t*-test, and χ^2-test were applied, when appropriate, to compare the differences between two groups. $P < 0.05$ was considered statistically significant.

Acknowledgments

We thank Drs Iain Bruce, Rui-Ping Xiao, Jincai Luo of Peking University, Drs Shey-Shin Sheu, Robert Dirksen of the University of Rochester, Dr Yuguang Shi of Pennsylvania State University and Dr Gerald Chan of Morningside Foundation for helpful discussions and critical comments. This work was supported by the Chinese National Natural Science Foundation, Major State Basic Research Development Programs of China (2011CB809100, 2007CB512100), Young Investigator Project (30800371) and National Institutes of Health of USA.

References

1 Houstis N, Rosen ED, Lander ES. Reactive oxygen species have a causal role in multiple forms of insulin resistance. *Nature* 2006; **440**:944-948.
2 Griendling KK, FitzGerald GA. Oxidative stress and cardiovascular injury: part II: animal and human studies. *Circulation* 2003; **108**:2034-2040.
3 Barnham KJ, Masters CL, Bush AI. Neurodegenerative diseases and oxidative stress. *Nat Rev Drug Discov* 2004; **3**:205-214.
4 Droge W. Free radicals in the physiological control of cell function. *Physiol Rev* 2002; **82**:47-95.
5 Foreman J, Demidchik V, Bothwell JH, *et al.* Reactive oxygen species produced by NADPH oxidase regulate plant cell growth. *Nature* 2003; **422**:442-446.
6 Owusu-Ansah E, Banerjee U. Reactive oxygen species prime *Drosophila* haematopoietic progenitors for differentiation. *Nature* 2009; **461**:537-541.
7 Newmeyer DD, Ferguson-Miller S. Mitochondria: releasing power for life and unleashing the machineries of death. *Cell* 2003; **112**:481-490.
8 Weissig V, Cheng SM, D'Souza GG. Mitochondrial pharmaceutics. *Mitochondrion* 2004; **3**:229-244.
9 Andrade FH, Reid MB, Allen DG, Westerblad H. Effect of hydrogen peroxide and dithiothreitol on contractile function of single skeletal muscle fibres from the mouse. *J Physiol* 1998; **509**:565-575.
10 Merry TL, Steinberg GR, Lynch GS, McConell GK. Skeletal muscle glucose uptake during contraction is regulated by nitric oxide and ROS independently of AMPK. *Am J Physiol Endocrinol Metab*; **298**:E577-E585.
11 Allen DG, Lamb GD, Westerblad H. Skeletal muscle fatigue: cellular mechanisms. *Physiol Rev* 2008; **88**:287-332.
12 Bonnard C, Durand A, Peyrol S, *et al.* Mitochondrial dysfunction results from oxidative stress in the skeletal muscle of diet-induced insulin-resistant mice. *J Clin Invest* 2008; **118**:789-800.
13 Gomes A, Fernandes E, Lima JL. Fluorescence probes used for detection of reactive oxygen species. *J Biochem Biophys Methods* 2005; **65**:45-80.
14 Robinson KM, Janes MS, Pehar M, *et al.* Selective fluorescent imaging of superoxide *in vivo* using ethidium-based probes. *Proc Natl Acad Sci USA* 2006; **103**:15038-15043.
15 Wang W, Fang H, Groom L, *et al.* Superoxide flashes in single mitochondria. *Cell* 2008; **134**:279-290.
16 Pouvreau S. Superoxide flashes in mouse skeletal muscle are produced by discrete arrays of active mitochondria operating coherently. *PLoS One* 2010; **5**: e13035.
17 Segretain D, Rambourg A, Clermont Y. Three dimensional arrangement of mitochondria and endoplasmic reticulum in the heart muscle fiber of the rat. *Anat Rec* 1981; **200**:139-151.
18 Vendelin M, Beraud N, Guerrero K, *et al.* Mitochondrial regular arrangement in muscle cells: a "crystal-like" pattern. *Am J Physiol Cell Physiol* 2005; **288**:C757-C767.
19 Ogata T, Yamasaki Y. Scanning electron-microscopic studies on the three-dimensional structure of sarcoplasmic reticulum in the mammalian red, white and intermediate muscle fibers. *Cell Tissue Res* 1985; **242**:461-467.
20 Misgeld T, Kerschensteiner M, Bareyre FM, Burgess RW, Lichtman JW. Imaging axonal transport of mitochondria *in vivo*. *Nat Methods* 2007; **4**:559-561.

21 Cai Q, Davis ML, Sheng ZH. Regulation of axonal mitochondrial transport and its impact on synaptic transmission. *Neurosci Res* 2011 Feb 23. doi:10.1016/j.neures.2011.02.005
22 Hollenbeck PJ. The pattern and mechanism of mitochondrial transport in axons. *Front Biosci* 1996; **1**:d91-d102.
23 DeFronzo RA, Jacot E, Jequier E, *et al.* The effect of insulin on the disposal of intravenous glucose. Results from indirect calorimetry and hepatic and femoral venous catheterization. *Diabetes* 1981; **30**:1000-1007.
24 Shulman GI, Rothman DL, Jue T, *et al*. Quantitation of muscle glycogen synthesis in normal subjects and subjects with non-insulin-dependent diabetes by 13C nuclear magnetic resonance spectroscopy. *N Engl J Med* 1990; **322**:223-228.
25 Luan B, Zhao J, Wu H, *et al.* Deficiency of a beta-arrestin-2 signal complex contributes to insulin resistance. *Nature* 2009; **457**:1146-1149.
26 Bakeeva LE, Chentsov Yu S, Skulachev VP. Mitochondrial framework (reticulum mitochondriale) in rat diaphragm muscle. *Biochim Biophys Acta* 1978; **501**:349-369.
27 Kirkwood SP, Munn EA, Brooks GA. Mitochondrial reticulum in limb skeletal muscle. *Am J Physiol* 1986; **251(3 Pt 1)**:C395-C402.
28 Kroemer G, Galluzzi L, Brenner C. Mitochondrial membrane permeabilization in cell death. *Physiol Rev* 2007; **87**:99-163.
29 Zoratti M, Szabo I. The mitochondrial permeability transition. *Biochim Biophys Acta* 1995; **1241**:139-176.
30 Erickson JR, Joiner ML, Guan X, *et al.* A dynamic pathway for calcium-independent activation of CaMKII by methionine oxidation. *Cell* 2008; **133**:462-474.
31 Schmid E, Hotz-Wagenblatt A, Hacj V, Droge W. Phosphorylation of the insulin receptor kinase by phosphocreatine in combination with hydrogen peroxide: the structural basis of redox priming. *FASEB J* 1999; **13**:1491-1500.
32 Loh K, Deng H, Fukushima A, *et al.* Reactive oxygen species enhance insulin sensitivity. *Cell Metab* 2009; **10**:260-272.

(**Supplementary information** is linked to the online version of the paper on the *Cell Research* website.)